Understanding the Macrosegregation Formation in Steel Ingot Castings: Examples of Multiphase Modeling

M. Wu, L. Könözsy, A. Fjeld, A. Ludwig
CD-Lab for Multiphase Modeling of Metallurgical Processes, Simulation and Modeling of Metallurgical Processes, Dept. Metallurgy, Univ. Leoben, A-8700, Austria

ABSTRACT: A multiphase modeling approach is employed to investigate the mechanisms which lead to macrosegregation. The following modeling examples are presented: feeding-induced macrosegregations in 1D unidirectional solidification situation, macrosegregations caused by thermosolutal buoyancy driven flow, macrosegregations caused by grain sedimentation, and macrosegregations which form in 3D mixed equiaxed-columnar solidification.

1. INTRODUCTION

Macrosegregation occurs due to the relative motion between the liquid and solid phases during solidification, which can arise as a result of thermosolutal convection, shrinkage induced flow, flotation and sedimentation, mechanical or electromagnetic stirring, flow induced by pore or gas bubble formation, deformation of the solid framework, or capillary force (Marangoni) induced flow. [1-5]. As summarized by Beckermann, "while some successes have been reported in predicting measured macrosegregation patterns in industrially relevant casting processes, there are still numerous areas where further development is required.[2]" The current report focuses on the authors' recent contributions to this topic via a discussion on the mechanisms and flow phenomena which cause macrosegregation. Four examples are presented, each highlighting particular aspects of flow phenomena which occur during solidification of a binary alloy. (i) Feeding induced macrosegregation, as studied by Flemings and others with the classical LSRE (local solute redistribution equation) model [6-8], is reproduced in a 1D unidirectional solidification model. (i) Macrosegregation due to thermosolutal buoyancy is modeled in a 2D axis-symmetric ingot with the assumption of columnar solidification. (iii) Macrosegregation due to grain sedimentation in the same 2D ingot casting is simulated with the assumption of globular equiaxed solidification. (iv) Lastly, macrosegregation occurring in a mixed equiaxed-columnar solidification model is investigated with the consideration of competitive crystal growth.

In the current paper a multiphase columnar, equiaxed, or mixed solidification model is used with a binary Fe-C alloy, 0.34 wt.%C. A simplified solidification path is assumed as a single primary solid phase with either columnar or globular equiaxed morphology. There is no distinction between ferrite and austenite phases. Details relevant to the numerical model and thermophysical and thermodynamic data are described in previous publications [9-10].

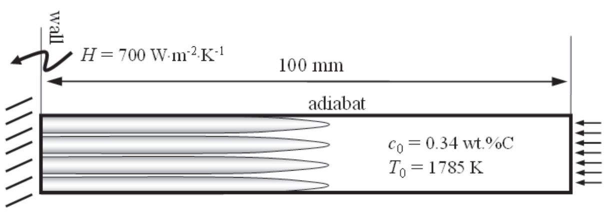

Fig. 1: Schematic of the benchmark of a 1D unidirectional solidification.

2. MODELING EXAMPLES AND DISCUSSIONS

2.1 Feeding-induced macrosegregations

The benchmark of a 1D unidirectional solidification, as shown in Fig. 1, is similar to the original case studied by Flemings et al.[6] and Kato et al.[8], and is often used to validate later numerical models [11]. Here we use the same case to validate the current multiphase model. In the model a constant heat transfer coefficient of 700 $W \cdot m^{-2} \cdot K^{-1}$ and a constant mold temperature of 300 K are applied on the left boundary, and a 'pressure inlet' condition with constant temperature of 1785 K is applied on the right boundary. Only two phases are considered, the melt and columnar dendrite trunks, and columnar dendrite morphology is approximated by step-wise growing cylinders. Solid and liquid densities are 7027 and 7424 kg·m^{-3}, respectively. The position of the growing columnar tip front is tracked explicitly [9]. Solidification shrinkage is the only mechanism to induce flow.

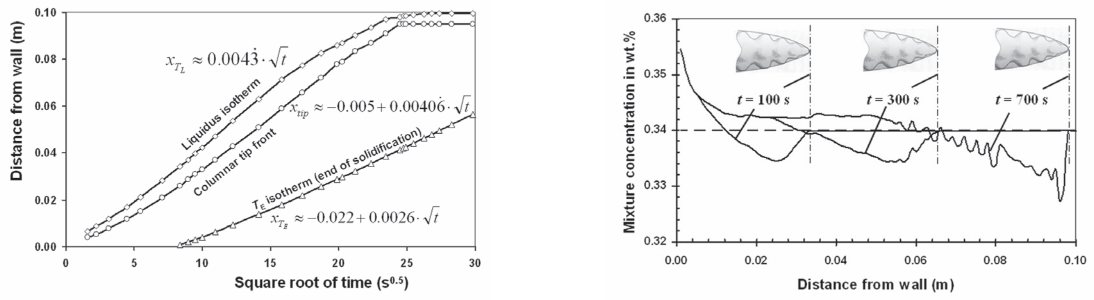

a) *b)*

Figure 2. Feeding induced macrosegregation in a 1D columnar solidifying configuration. a) Calculated position of liquidus isotherm, columnar tip front and eutectic isotherm as function of the square root of time; b) Schematic of the columnar tip front position and the predicted macrosegregation (c_{mix} in wt.%C) development at different instants in time.

As shown in Fig. 2(a), the simulation results show typical unidirectional solidification from a cold mold with finite thermal resistance at the metal/mold interface. Fig. 2(b) shows c_{mix}, the local concentration of solute, along the sample at three instants in time. Each curve is a snapshot of the macrosegregation in the sample over the course of solidification. It indicates a region of positive segregation in the sample, followed by a region of negative segregation. This negative segregation (c_{mix} smaller than nominal concentration c_0) corresponds to the region behind the columnar tip front. This pattern of positive and negative segregation is caused by feeding due to solidification shrinkage. The solute-rich melt in the mushy region is transported to the root of the dendrite trunks to fill the solidification shrinkage, and correspondingly fresh melt ($c_l = c_0$) is drawn into the mushy zone from the bulk liquid ahead of the columnar tips. At the end (700 s) it predicts maximum positive segregation (inverse segregation) at the mold surface, slightly positive segregation along the sample, and negative segregation at the end of the sample. Negative segregation can only occur at the end of solidification, when feeding is insufficient. These results agree with Flemings' analytical solution and other experimental findings [6, 8].

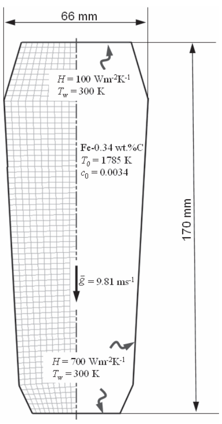

Fig. 3: Schematic of a reduced steel ingot.

2.2 Thermosolutal convection-induced macrosegregation

Solidification of a steel ingot (Fig. 3) is simulated with a 2D axisymmetric model. Again a two-phase columnar solidification configuration is considered with an initial bulk melt concentration of Fe-0.34 wt.%C and an initial temperature of 1785 K. Mold filling is not considered. Values for heat transfer coefficients, mold and air temperatures are constant and are shown in Fig. 3. Two phases are considered, the melt and columnar dendrite trunks; columnar dendrite morphology is approximated by step-wise growing cylinders. The columnar trunks grow from side and bottom walls, and the columnar tip front is tracked explicitly. A Boussinesq approximation is used to treat thermosolutal convection, the thermal and solutal expansion coefficients of the melt are $\beta_T = 2.x10^{-4}$ K^{-1}, and $\beta_c = 0.011$ wt.%$^{-1}$, respectively.

The solidification sequences and evolution of c_{mix} are shown in Fig.4 a)-d). The columnar tip front and the volume fraction of columnar phase (f_c-isolines) move from the mold wall towards the bulk melt region. Due to thermosolutal convection, the 'hot spot' moves upwards and is solidified slightly above the center of the casting. During solidification an axisymmetric convection pattern develops. The melt near the mold wall has a higher density due to its lower temperature, and thus sinks downwards, while the hotter melt in the center rises. One may argue that the solute-enriched, lower density interdendritic melt might rise and thus partially compensate or reverse the above mentioned convection pattern. However, with the given temperature gradient, thermal buoyancy dominates over solutal buoyancy. The downward flow near the columnar tip region and the upward flow in the bulk melt are the primary phenomena which lead to the final macrosegregation.

The final macrosegregations for the benchmark are predicted as shown in Fig. 4e): A small region with negative macrosegregation ($c_{mix} < c_0$) is found in the upper surface region, particularly in the upper corners where c_{mix}~0.33; In the lower corners a positive macrosegregation is predicted c_{mix}~0.36; A large area of positive macrosegregation with $c_{mix} > 0.38$ is located in the casting center.

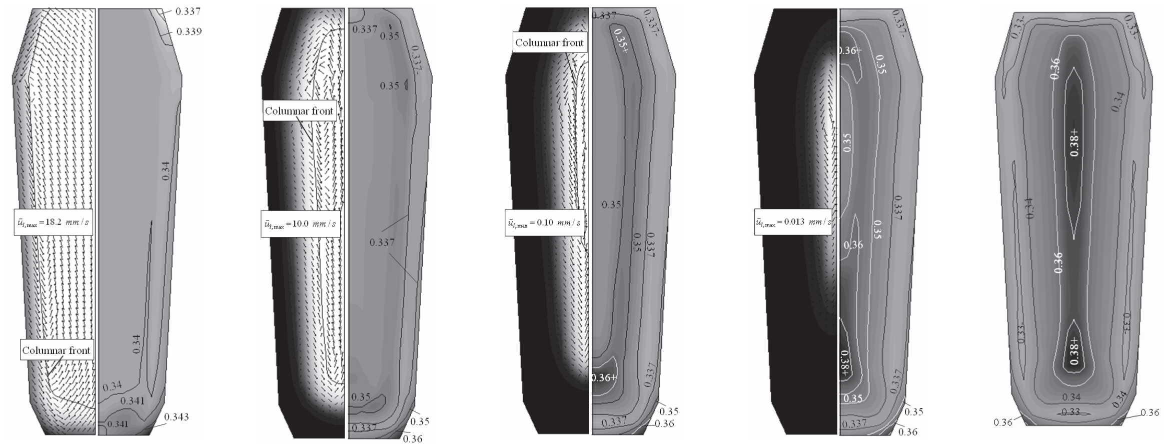

a) at 2 s *b) at 30 s* *c) at 50 s* *d) at 67 s* *e) final c_{mix}*

Fig. 4: Predicted solidification sequence and macrosegregation formation induced by thermosolutal convection in the reduced steel ingot. The left half of a)-d) shows the volume fraction evolution of the columnar phase in gray scale with the columnar tip position indicated with a solid line, and overlaid with the melt velocity. The right half of the series shows the evolution of the c_{mix} pattern, gray-scaled according to positive and negative segregation. The predicted final macrosegregation pattern is shown in figure e).

In the upper corner, the interdendritic melt flows through the stationary columnar trunks. The melt flows into the corner horizontally, and it flows out of the corner vertically along the side wall. The melt flowing out of the corner, with a relative high concentration, is replaced with 'almost-fresh' melt of near bulk concentration. This results in a decrease in c_{mix} in the corner region and a corresponding negative macrosegregation. In the lower bottom corner, the melt flowing vertically into the corner is enriched in solute due to segregation in the solidifying interdendritic region along the mold wall. As the solidification now takes place from that enriched melt, the solid forms with a higher concentration, thus creating positive macrosegregation. Positive macrosegregation in the center (Fig. 4) is formed gradually during solidification. As mentioned above, the interdendritic melt has a higher concentration than the bulk melt. The interdendritic solute-enriched melt is brought out of the mushy zone by the flow current, causing c_{mix} in front of or slightly behind the columnar tip front to be enriched gradually. These solute enriched melts are not stationary, they move with the flow current, and finally meet in the casting center and form a large positive segregation zone.

2.3 Sedimentation-induced macrosegregation

Solidification of previous ingot benchmark (Fig. 3) is again simulated with a 2D axisymmetric model, but now with the assumption of globular equiaxed solidification. Solidification begins with an initial melt concentration of Fe-0.34 wt.%C and an initial temperature of 1785 K. The values of heat transfer coefficients, mold and air temperatures shown in Fig. 3 are used. The two phases considered are the melt and globular equiaxed grains where the grain morphology is approximated as spheres. The spherical grains in the bulk melt can move freely up to a 'packing limit' of f_s^c=0.637. A three-parameter ($n_{\max} = 1\times10^{11}\ \mathrm{m^{-3}}$, $\Delta T_\sigma = 4\ \mathrm{K}$, $\Delta T_\mathrm{N} = 10\ \mathrm{K}$) heterogeneous nucleation law is used for the nucleation. A Boussinesq approximation is used to treat buoyancy flow and grain sedimentation and solid and liquid densities are 7027 and 7321 kg·m^{-3}, respectively.

Evolution sequences of the equiaxed phase, the sedimentation, and the induced macrosegregation phenomena are shown in Fig. 5. At the initial stage, grains which nucleate in the upper regions and at the side walls sink downwards. The sinking grains drag the surrounding melt with them, creating a downward flow of melt at the wall and a corresponding upward flow in the casting center. As a result, an axisymmetric melt convection roll develops in the melt. Within this induced melt flow, however, the relative velocity of equiaxed grains to the melt, $\vec{u}_\mathrm{e} - \vec{u}_\mathrm{l}$, always points downwards. The sinking grains lead to an accumulation of solid in the bottom region of the casting and cease to move when the local fraction of solid exceeds the packing limit. Events such as grain nucleation, grain growth and sedimentation continue until the final stages of solidification. The 'hot spot' in the casting is very close to the surface due to the small heat transfer coefficient at the casting top surface.

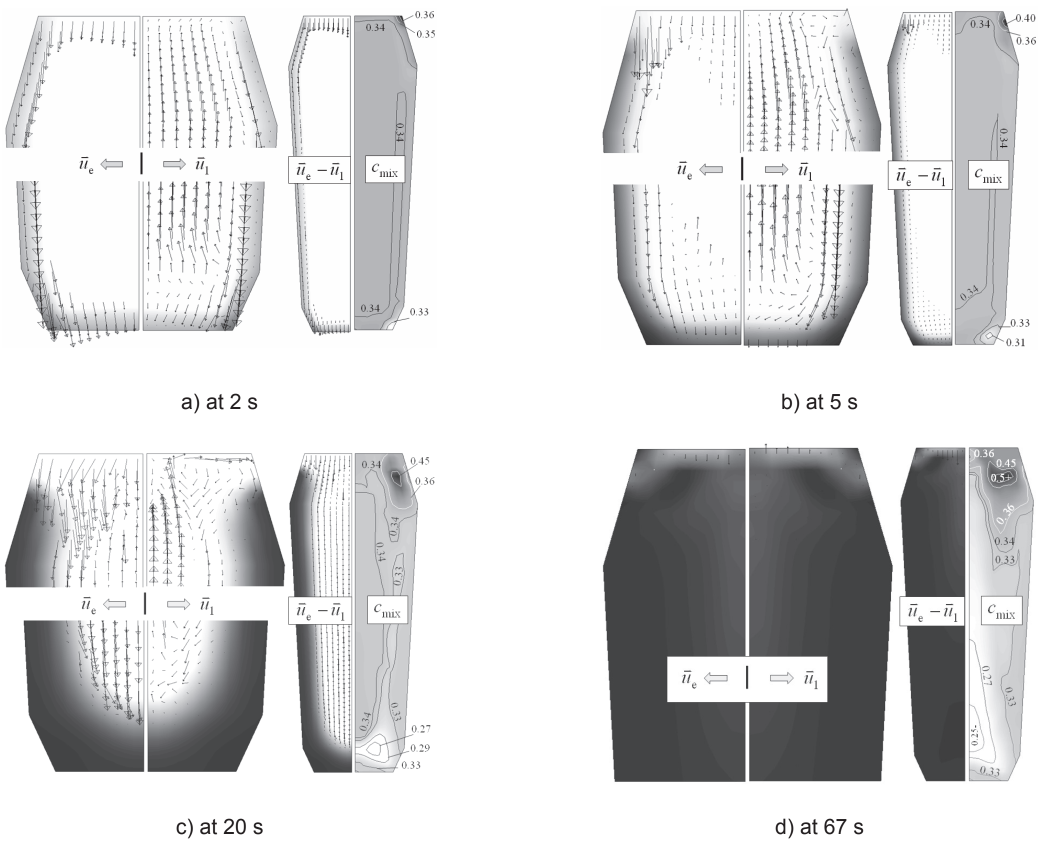

a) at 2 s

b) at 5 s

c) at 20 s

d) at 67 s

Fig. 5. Predicted solidification sequence and formation of macrosegregation induced by grain sedimentation. The volume fraction of equiaxed grains f_e is shown in gray-scale (light for f_e = 0 and dark for f_e = 1), and overlaid with the equiaxed velocity $\vec{u}_\mathrm{e}$, melt velocity $\vec{u}_\mathrm{l}$, and the relative velocity $\vec{u}_\mathrm{e} - \vec{u}_\mathrm{l}$. The distribution of c_{mix} is also shown in gray-scale. The final macrosegregation pattern is almost identical to the one at 67 s.

The relative motion between the equiaxed grains and the melt is a primary cause of macrosegregations. They occur via two mechanisms: (a) the replacement of the solute rich melt by solute poor grains and (b) the replacement of the solute poor grains by the solute rich melt. The mechanism (a) leads to negative segregation, while mechanism (b) leads to positive segregation. As shown in Fig. 5, in the initial stage the solute-poor grains in the top corner regions sink along the mold wall and fresh melt is drawn horizontally into the corners, i.e. mechanism (b), causing positive segregation. In the bottom corner, the solute-poor grains settle and 'squeeze' the solute-enriched melt out of the corner, causing negative segregation. In the top corner the positive segregation zone is actually not stationary. It moves downwards along the wall, then moves slowly away from the wall, towards the casting center. This is of course due to the fact that the positive segregation zone is within the fluid region and thus moves with the flow currents in the melt. As is evident in Fig. 5 b)-c), the melt flows continuously into the corner along the casting top surface, where a local circulation current develops, which causes the positive segregation region to move. This positive zone, as it moves, becomes wider and wider. The grains continue to grow, sink, and eventually leave the enriched melt behind. While sedimentation goes on, the bottom negative segregation zone becomes larger and larger as well. The grains pile-up slowly, creating a relatively large negative segregation zone at the bottom. The mixture concentration field is slightly modified in the last stages of solidification, due to the coupling of melt flow and grain movement. However, the primary mechanism responsible for negative segregation at the bottom of the casting is due to mechanism (a).

2.4 Macrosegregation in mixed columnar-equiaxed solidification

A 3D, mixed columnar-equiaxed model is used to simulate solidification of the same benchmark shown in Fig. 3. Macrosegregation formation due to the combined appearance of thermosolutal convection, grain sedimentation, and sedimentation induced convection is investigated with this model. Solidification begins with an initial concentration Fe-0.34 wt.%C and an initial temperature of 1785 K. Values for heat transfer coefficients, mold and air temperatures are considered constant as indicated in Fig. 3. Three phases are considered: the melt, globular equiaxed grains and columnar dendrite trunks. Morphologies are approximated by step-wise growing cylinders for columnar dendrite trunks and spheres for globular equiaxed grains. The columnar trunks grow from side and bottom walls, and the columnar tip front is explicitly tracked. A three-parameter heterogeneous nucleation law is used for the nucleation of the equiaxed grains: $n_{\max} = 5\times10^{9}\ \mathrm{m}^{-3}$, $\Delta T_{\sigma} = 2\ \mathrm{K}$, $\Delta T_{\mathrm{N}} = 5\ \mathrm{K}$. The grains ahead of the columnar tip front can move if the equiaxed volume fraction is below the "packing limit," $f_s^c = 0.637$. Hunt's blocking mechanism is applied for predicting CET [12]. Fragmentation and grain attachment are currently not considered. The buoyancy force of the moving grains and the thermosolutal convection are accounted for by a Boussinesq approximation and shrinkage flow is ignored.

The solidification sequences, including sedimentation of the globular equiaxed grains, the sedimentation-induced and thermosolutal buoyancy-induced melt convection, are shown in Fig. 6(a). The solidification pattern agrees with the classical explanation of steel ingot solidification, summarized by Campbell [13]. The columnar dendrites grow from the mold wall and the columnar tip front moves inwards. The equiaxed grains nucleate near the mold walls and in the bulk melt. The columnar dendrites are stationary, whereas the equiaxed grains sink and settle in the base of the ingot. The accumulation of such grains at the base of the ingot has a characteristic cone-shape. The sedimentation of grains and the melt convection influence the macroscopic solidification sequence and thus, the final phase distribution. More equiaxed grains will be found at the bottom and in the base region, while columnar solidification will be predominant in the upper part of the ingot.

As the columnar tip front is explicitly tracked, the simulation shows that the columnar tip fronts from both sides tend to meet in the casting center. However, in the lower part of the casting the large amount of equiaxed grains stops the propagation of the columnar tip front. Its final position indicates the CET position. The CET separates areas where only equiaxed grains appear from areas where both columnar dendrites and equiaxed grains might coexist.

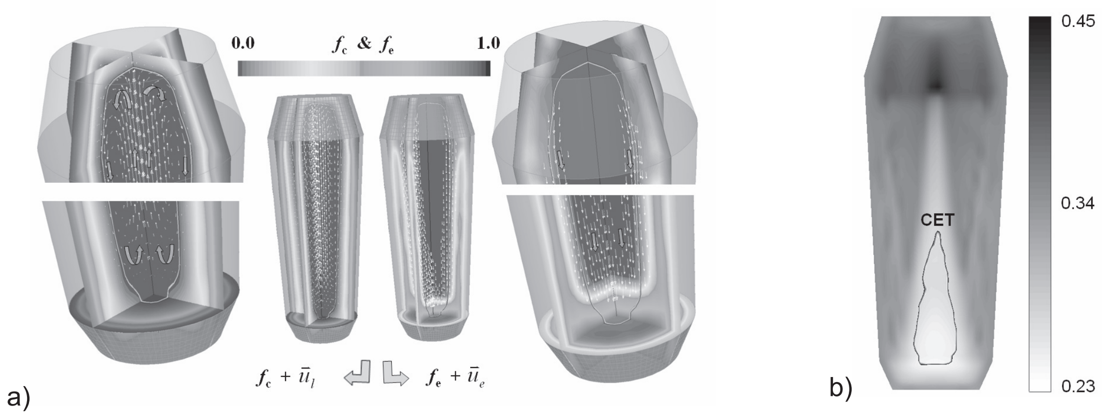

Fig. 6: a) Simulated solidification sequence (at 20 s) of the steel ingot. f_c and f_e are shown in color in two vertical and one horizontal sections, the velocity fields $\vec{u}_l$ and $\vec{u}_e$ are shown as vectors. The columnar tip front position is also shown. b) Predicted mix concentration c_{mix} in the steel ingot, scaled from 0.23 wt.% C (light) to 0.45 wt.% C (dark). The area of 100% equiaxed macrostructure is surrounded by the CET line.

The final macrosegregation distribution is predicted, as shown in Fig. 6(b). From the simulation results it appears obvious that the main mechanism for the cone-shaped negative segregation in the base region is grain sedimentation. The settling grains are poor in solute elements, thus their pile-up results in negative segregation in the bottom of the ingot. A further contributing factor to the strength of negative segregation arises from the flow divergence of the residual liquid through this zone at a late solidification stage. The positive segregation at the top region of the ingot is caused by the flow of the enriched melt in the bulk region. This kind of positive segregation coincides with classical experimental results [13]. It should be noted that channel segregations, which are frequently found in steel ingots, are not expected in such a reduced ingot.

3. SUMMARY

Through the four modeling examples presented here, 1D unidirectional solidification, 2D columnar, 2D equiaxed, and a full 3D mixed columnar-equiaxed solidification model, the flow phenomena which lead to specific macrosegregation patterns in each model have been dissected and discussed. Particularly the variety of flow patterns, relative motion between the liquid and solid phases, and their competing influences have been explained in detail to give the reader an understanding of the final macrosegregation patterns commonly found in many castings and ingots. Although the models discussed here are qualitative in nature as a result of the model assumptions and simplifications, thus deviating from some industrial castings, it is clear that multiphase modeling is a powerful tool which can provide deeper insight into complex macrosegregation phenomena. Future work will include the necessary refinements required to successfully create sophisticated multiphase models compatible with industrial castings.

4. REFERENCES

[1] M.C. Flemings, ISIJ Intern., 40(2000), 833.

[2] C. Beckermann, Int. Mater. Rev., 47(5)(2002), 243.

[3] G. Lesoult, Mater. Sci. Eng. A, 413-414(2005), 19.

[4] I. Ohnaka, Metals Handbook, 15: Castings, (USA: ASM International, 1998), 136.

[5] M. Wu, A. Ludwig, Adv. Eng. Mater., 7(9)(2005), 846.

[6] M.C. Flemings, G.E. Nereo, Trans. TMS-AIME, 239(1967), 1449.

[7] M.C. Flemings, G.E. Nereo, Trans. TMS-AIME, 242(1968), 50.

[8] H. Kato, J.R. Cahoon, Metall. Trans., 16A(1985), 579.

[9] M. Wu, A. Ludwig, Metall. Mater. Trans., 37A (2006), 1613.

[10] A. Ludwig, M. Wu, Mater. Sci. Eng. A, 413-414(2005), 109.

[11] V.R. Voller, S. Sundarraj, Int. J. Heat Mass Transfer, 38(6)(1995), 1009.

[12] J. D. Hunt, Mater. Sci. Eng., 65(1984), 75.

[13] J. Campbell, Castings, (Butterworth Heinemann Ltd, Oxford, 1991), 151-158.